Published OnlineFirst June 30, 2011; DOI:10.1158/0008-5472.CAN-11-0412

Cancer Research

Analysis of Mitosis and Antimitotic Drug Responses in Tumors by *In Vivo* Microscopy and Single-Cell Pharmacodynamics

James D. Orth, Rainer H. Kohler, Floris Foijer, et al.

Cancer Res 2011;71:4608-4616. Published OnlineFirst June 30, 2011.

Updated Version	Access the most recent version of this article at: doi:10.1158/0008-5472.CAN-11-0412
Supplementary Material	Access the most recent supplemental material at: http://cancerres.aacrjournals.org/content/suppl/2011/06/24/0008-5472.CAN-11-0412.DC1.html

Cited Articles	This article cites 40 articles, 8 of which you can access for free at: http://cancerres.aacrjournals.org/content/71/13/4608.full.html#ref-list-1
Citing Articles	This article has been cited by 3 HighWire-hosted articles. Access the articles at: http://cancerres.aacrjournals.org/content/71/13/4608.full.html#related-urls

E-mail alerts	Sign up to receive free email-alerts related to this article or journal.
Reprints and Subscriptions	To order reprints of this article or to subscribe to the journal, contact the AACR Publications Department at pubs@aacr.org.
Permissions	To request permission to re-use all or part of this article, contact the AACR Publications Department at permissions@aacr.org.

Downloaded from cancerres.aacrjournals.org on July 19, 2012
Copyright © 2011 American Association for Cancer Research

Published OnlineFirst June 30, 2011; DOI:10.1158/0008-5472.CAN-11-0412

Cancer Research

Analysis of Mitosis and Antimitotic Drug Responses in Tumors by *In Vivo* Microscopy and Single-Cell Pharmacodynamics

James D. Orth[1], Rainer H. Kohler[2], Floris Foijer[1,3], Peter K. Sorger[1], Ralph Weissleder[1,2], and Timothy J. Mitchison[1]

Abstract

Cancer relies upon frequent or abnormal cell division, but how the tumor microenvironment affects mitotic processes *in vivo* remains unclear, largely due to the technical challenges of optical access, spatial resolution, and motion. We developed high-resolution *in vivo* microscopy methods to visualize mitosis in a murine xenograft model of human cancer. Using these methods, we determined whether the single-cell response to the antimitotic drug paclitaxel (Ptx) was the same in tumors as in cell culture, observed the impact of Ptx on the tumor response as a whole, and evaluated the single-cell pharmacodynamics (PD) of Ptx (by *in vivo* PD microscopy). Mitotic initiation was generally less frequent in tumors than in cell culture, but subsequently it proceeded normally. Ptx treatment caused spindle assembly defects and mitotic arrest, followed by slippage from mitotic arrest, multinucleation, and apoptosis. Compared with cell culture, the peak mitotic index in tumors exposed to Ptx was lower and the tumor cells survived longer after mitotic arrest, becoming multinucleated rather than dying directly from mitotic arrest. Thus, the tumor microenvironment was much less proapoptotic than cell culture. The morphologies associated with mitotic arrest were dose and time dependent, thereby providing a semiquantitative, single-cell measure of PD. Although many tumor cells did not progress through Ptx-induced mitotic arrest, tumor significantly regressed in the model. Our findings show that *in vivo* microscopy offers a useful tool to visualize mitosis during tumor progression, drug responses, and cell fate at the single-cell level. *Cancer Res; 71(13); 4608–16. ©2011 AACR.*

Introduction

The bulk of cancer cell biology has been conducted using *in vitro* systems, with cells cultured in artificial environments. To better understand the origin and progression of cancer and chemotherapeutic drug responses, we need *in vivo* imaging data, ideally at the single-cell level. Whole-body imaging methods, including optical, MRI, positron emission tomography (PET), and computed tomography (CT) scans, report on the state of tissues and diseases but generally lack the resolution required for single-cell analysis (1). High-resolution images can be obtained from histology, but this requires invasive biopsies or sacrificing animals at each time point, without providing real-time data. Live cell imaging in culture has revealed dynamic aspects of cancer cell biology and drug responses of single cells, but how these data apply to the situation *in vivo* is largely unknown. Thus, a clear need exists for subcellular resolution intravital microscopy (IVM) to correlate the acute responses of cells to drugs with the ultimate fates of cells, tumors, and tissues in animal models of human disease. In rodents, IVM typically involves a glass window set into the animal, or an exteriorized organ (2–5), to directly observe underlying tissues and tumors (6–9). In optically favorable organisms such as zebra fish, drosophila, and nematodes, IVM can visualize dynamic processes at the single-cell level (10–12). But most applications of IVM in rodents follow cells or groups of cells at relatively low resolution. The challenges facing subcellular IVM include physiologic motion, low signal to noise ratios, and slow image capture rates that limit directly studying rapid intracellular processes and transient events at a quality comparable with culture systems. Overcoming these limitations requires addressing issues including light penetration, phototoxicity, and especially motion caused by breathing, heartbeat, and muscle movements. Here, we report optimized IVM that enables highly detailed, subcellular light microscopy to study formation of the mitotic spindle and chromosome dynamics before and after drug delivery in xenograft tumors (Fig. 1A–C). Using this *in vivo* pharmacodynamic microscopy (IPDM), we analyzed the response of paclitaxel (Ptx), an important anticancer mitotic drug,

Authors' Affiliations: [1]Department of Systems Biology, Harvard Medical School; [2]Center for Systems Biology, Massachusetts General Hospital, Boston, Massachusetts; and [3]Wellcome Trust Sanger Institute, Wellcome Trust Genome Campus, Hinxton, United Kingdom

Note: Supplementary data for this article are available at Cancer Research Online (http://cancerres.aacrjournals.org/).

Corresponding Author: James D. Orth, Department of Systems Biology, WAB541, Harvard Medical School, 200 Longwood Ave, Boston, MA 02115. Phone: 617-432-3728; Fax: 617-432-5012; E-mail: james_orth@hms.harvard.edu

doi: 10.1158/0008-5472.CAN-11-0412

©2011 American Association for Cancer Research.

American Association for Cancer Research

Downloaded from cancerres.aacrjournals.org on July 19, 2012
Copyright © 2011 American Association for Cancer Research

Published OnlineFirst June 30, 2011; DOI:10.1158/0008-5472.CAN-11-0412

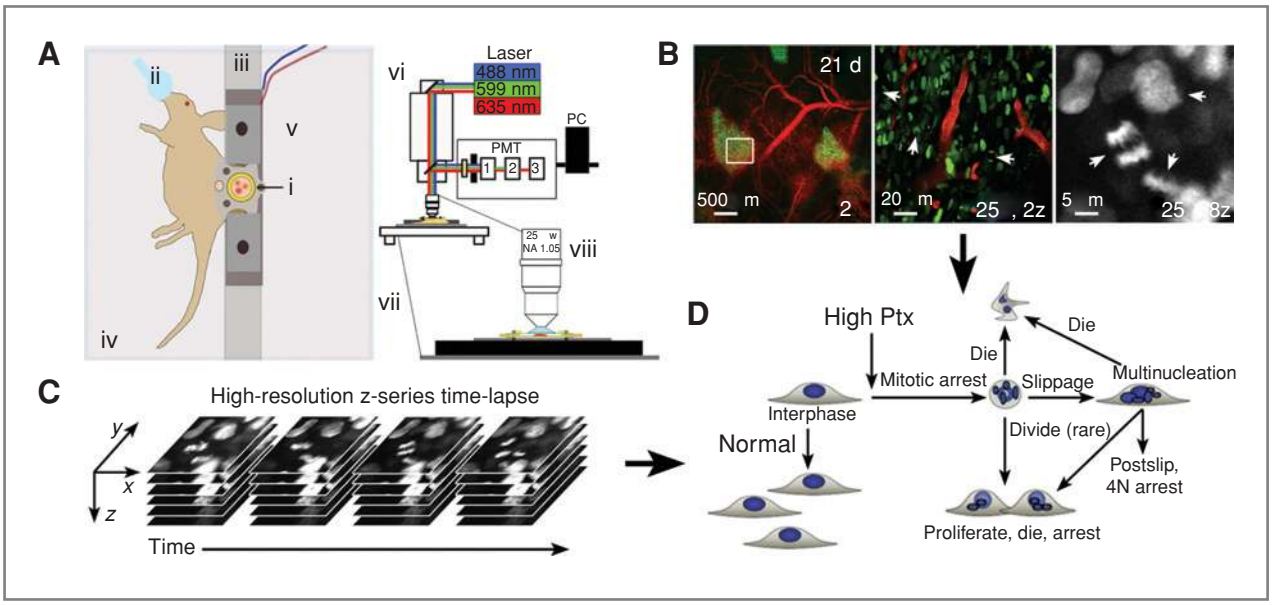

Figure 1. IPDM. A, the imaging system. Xenograft tumor(s) in the DSC (i); anesthesia (ii); temperature-regulated holding bar (iii); temperature-regulated stage (iv); DSC holding plate and finger screws (v); laser scanning confocal microscope (vi); charged air table (vii); objective (viii). PC, personal computer. B, HT-1080 tumor–expressing H2b–EGFP (green) with Angiosense-680–labeled blood vessels (red). Microscopy at different resolutions allows for the identification of mitotic profiles (arrows) and specific mitotic stages (arrows). 2z, 25× lens; 2× zoom. 8z, 25× lens; 8× zoom. C, z-series time-lapse microscopy. D, in culture, the Ptx response shows high intra–cell line variability. After mitotic arrest, cells can progress along multiple pathways. Both z-series imaging (B) and z-series time-lapse microscopy (C) were used to study mitosis and Ptx response.

whose biology remains poorly understood at the whole-tumor level.

Mitosis is central to tumor growth, and aneuploidy due to mitotic errors contributes to both tumorigenesis and the progression of cancer toward more aggressive genotypes (13). Antimitotic drugs that perturb microtubule dynamics are part of the chemotherapy regime for treating many cancers, and experimental drugs against other mitotic spindle proteins are in clinical trials (14). Ptx binds to microtubules, interferes with polymerization dynamics, promotes mitotic arrest, and triggers apoptosis in cancer cells (15–18). Time-lapse microscopy in culture has revealed important aspects of Ptx response dynamics and significant intracellular variability (Fig. 1D; ref. 19). At saturating Ptx concentrations (typically 100–300 nmol/L), cells rarely die without first entering mitotic arrest that can last 24 hours or longer depending on the cell line (19). Postarrest, cells either initiate apoptosis or exit without dividing into an abnormal G_1-like state with multiple small nuclei; this abnormal mitotic exit is termed mitotic slippage (Fig. 1D; ref. 20). Once multinucleated, most cells cannot recover normal nuclear morphology and remain arrested, die, or attempt another mitosis that is typically multipolar (e.g., tripolar and not bipolar). Which of these pathways a given cell follows is highly variable both within a cell line and between cell lines (19, 21).

Although the effects of Ptx on microtubules and mitosis are well understood in culture (22, 23), many questions remain as to how it promotes tumor regression *in vivo*, why patients with the same diagnosis respond differently, and how resistance arises (24). One basic question is whether Ptx kills only cells that have entered mitosis in tumors, as in culture, that is, is Ptx solely an antimitotic drug in the tumor context? Pharmacokinetic (PK; drug concentration vs. time) and PD (drug action vs. time) data are essential for understanding tumor responses. In contrast to the extensive information on the PK of Ptx (18, 25–27), its PD is complicated and requires better understanding via a development of biomarkers, ideally at multiple sequential steps in the drug action pathway. Two natural biomarkers for Ptx are mitotic arrest and cell death. These have been used as PD biomarkers in human and rodent cancer models by scoring histology sections or stained biopsies (16, 28–30); multinucleation has been largely ignored. A dynamic readout of these biomarkers would be more powerful, especially if it could be calibrated to measure the relative Ptx concentration experienced by a tumor cell as a function of dose and time. Effects of Ptx on the morphology and duration of mitosis are concentration dependent in cell culture (31, 32), suggesting these measurements might provide semiquantitative PD biomarkers in tumors. At low concentrations in culture ($\leq$5 nmol/L), mitosis is delayed and often exhibits errors in chromosome alignment and segregation; at moderate concentrations (5–20 nmol/L), mitotic delays are longer and cells often exhibit spindle multipolarity and multipolar division; at high concentrations (>20 nmol/L), cells arrest for many hours and then die or slip. These concentration-dependent responses have not been studied *in vivo*.

The questions we sought to answer included the following: (i) Can tumor cells be visualized at a high enough resolution to observe single-chromosome errors during mitosis and to discriminate different morphologic biomarkers of Ptx action? (ii) How do Ptx responses differ in culture and in tumors, and are all Ptx effects in tumors mediated via mitotic arrest?

Downloaded from cancerres.aacrjournals.org on July 19, 2012
Copyright © 2011 American Association for Cancer Research

Published OnlineFirst June 30, 2011; DOI:10.1158/0008-5472.CAN-11-0412

(iii) Can we quantify PD for a small-molecule drug using live, subcellular imaging? To address these questions, human tumor cell lines known to establish xenograft tumors in nude mice were engineered to stably express fluorescent protein fusions to histone H2b (to visualize chromatin) and/or β1-tubulin (to visualize microtubules). These cell lines report on cell-cycle state (interphase or mitotic), spindle morphology, mitotic errors such as lagging chromosomes, mitotic arrest, passage through mitotic arrest, and apoptosis. We used dorsal skinfold chambers (DSC) and developed multiple approaches for immobilization and stabilization. Figure 1A depicts the main features of the setup. HT-1080 cells rapidly established vascularized tumors in DSCs (Fig. 1B). Imaging with a 2× objective revealed overall tumor morphology and blood vessels, whereas our standard imaging conditions revealed detailed morphology (Fig. 1B).

Materials and Methods

Mice

Mice were housed and handled according to Harvard Medical Area Institutional Animal Care and Use Committee guidelines. Nu/Nu mice (Cox-7; Massachusetts General Hospital, Boston, MA) were anesthetized for DSC implantation by intraperitoneal (i.p.) injection of a 1:10 mixture of ketamine (50 mg/mL; Bioniche Pharma) and xylazine (100 mg/mL; Vedco, Inc.) or by isoflurane vaporization (Harvard Apparatus) at a flow rate of 2.0 L/min isoflurane:2.0 L/min oxygen. For cell injection, injection of Ptx, and microscopy, mice were anesthetized by 2.0 L/min isoflurane:2.0 L/min oxygen. For more than 1 hour of imaging, the isoflurane flow rate was slowly reduced to 0.8 to 1.2 L/min. Surgeries were conducted under sterile conditions with a zoom stereomicroscope (Olympus SZ61).

DSC implantation

Titanium DSCs (APJ Trading Co, Inc.) were implanted into the dorsal skinfold of Nu/Nu mice as described (2, 3, 7, 33). The DSC stretches and sandwiches the 2 layers of skin on the back of the mouse. On one side, the skin is surgically removed and replaced by a 10-mm-diameter optical glass cover slip held in place with a c-clip. Spacers between the both halves of the DSC frame prevent excess compression of the tissue and vessels. The window allows free-access imaging of the remaining layers of striated skin muscle, s.c. tissue, deep dermis, and tumors.

Cell injection into DSC

Cells were harvested by trypsinization (0.25% trypsin-EDTA) and resuspended in growth medium. Mice were anesthetized and approximately 10^6 (50 μL) cells were injected s.c. using a 0.5-mL insulin syringe ($28^1/_2$G; BD Biosciences). The needle was bent at 90 degrees to aid injection. Injections were carried out under a stereomicroscope. After injection, sterile saline was added into the DSC and it was closed with a new cover slip. For orientation and to establish a baseline for tumor growth, the cell mass was imaged 1 to 2 days after injection. Tumors were rejected if there were any gross tissue abnormalities. The procedures resulted in no mortality and more than 95% of DSCs were adequate for microscopy. To evaluate and refine IVM methods, HeLa and U2OS cells (which did not establish tumors in DSCs) were injected, with or without Ptx or Kinesin-5 inhibitor (K5I) pretreatment in culture, and imaged within 7 days.

Ptx and K5I treatment

To allow neovascularization, HT-1080 xenografts were grown for 8 days or more before Ptx treatment. Mice were injected in tail vein with a single bolus of 1.2, 3, 6, or 30 mg/kg Ptx (injectable formulation, Novaplus; Bedford Laboratories), diluted 1:4 with saline. A total of 30 mg/kg Ptx was used as the high dose according to published data (29, 34, 35). K5I EMD534085 (36) was from Merck Serono and was used in culture at 500 nmol/L.

Microscopy

To reduce motion artifacts and permit high-resolution microscopy over extended periods, a DSC holder was designed (Fig. 1A). The setup consists of an aluminum holder attached to an aluminum platform. The platform and DSC holder were kept at 38°C to reduce thermal drift. The screws of the DSC fit into machined holes in the holder and the DSC frame was further immobilized using small plates and screws. A charged air table reduced vibration external to the instrumentation. Two hundred microliters of saline was injected i.p. every hour during imaging to maintain hydration. For vascular imaging, fluorescein isothiocyanate–dextran [molecular weight (MW) = 2,000,000; Sigma-Aldrich] or Angiosense-680 (MW = 250,000; PerkinElmer, Inc.) was injected tail vein. A customized Olympus FV1000 based on a BX61-WI confocal microscope was used. Olympus objectives were as follows: 25× XPlan N [numerical aperture (NA) = 1.05, water], 2×/340 XLFluor (NA = 0.14, air), 20× UPlanFL (NA = 0.50), and 60× LUMFL N (NA = 1.10, water). Enhanced green fluorescent protein (EGFP), monomeric red fluorescent protein (mRFP), TagRFP, and Angiosense-680 were excited using a 488-nm argon ion laser line, 559-nm pumped solid-state laser, or 635-nm diode laser, respectively, in combination with a DM405/488/559/635-nm dichroic beam splitter. Emitted light was separated and collected with beam splitters SDM560 and SDM640 and band-pass filters BA505-540, BA575-620, and BA655-757. Control tumors were used to optimize imaging conditions resulting in no photobleaching or phototoxicity. Using a motorized *x*–*y* stage, 5 z-stack time series with 10 to 20 optical sections (5 μm per section), at 30 seconds to 5 minutes intervals, were collected. Small drifts in focus were corrected in real time, using the z-adjustment feature of FluoView 1000 software.

Results

Visualization of detailed mitotic morphology *in vivo*

We used HT-1080 cells in all experiments but confirmed general concepts by using HeLa and U2OS. HeLa cells expressing both H2b-mRFP and mEGFP–α-tubulin were used to convey chromosomes and the mitotic spindle simultaneously (Fig. 2). Progression through normal mitosis was readily observed (Fig. 2A–D; Supplementary Movie 1). At higher

Downloaded from cancerres.aacrjournals.org on July 19, 2012
Copyright © 2011 American Association for Cancer Research

Published OnlineFirst June 30, 2011; DOI:10.1158/0008-5472.CAN-11-0412

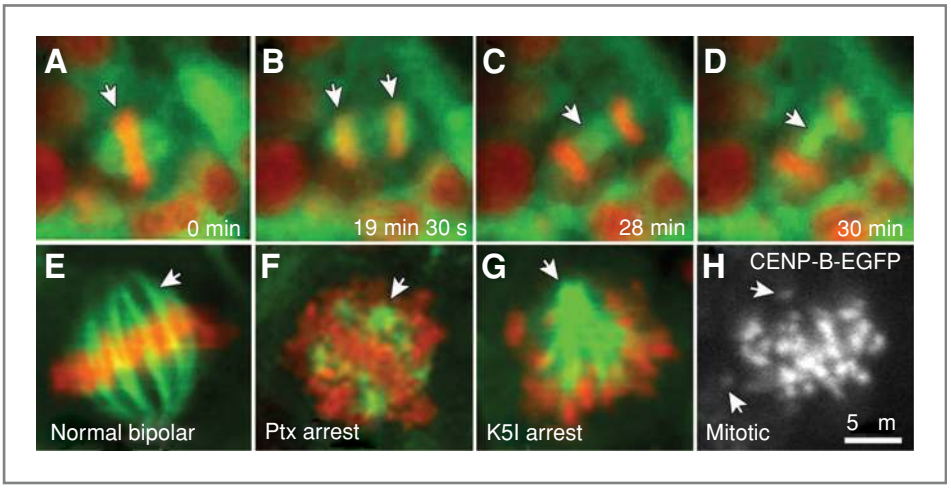

Figure 2. Mitosis and mitotic spindle structures via IPDM. A–D, HeLa H2b-mCherry/tubulin–EGFP cells. All stages of mitosis can be observed. See Supplementary Movie 1. Arrows (A and B), chromosomes. Arrows (C and D), microtubule midzone. E, normal mitotic cell at higher magnification reveals kinetochore fibers (arrow). F and G, different antimitotic drug-induced phenotypes. F, Ptx-arrested mitotic cell showing microtubule rosettes surrounded by chromosomes (arrow). G, K5I-arrested mitotic cell showing monopolar spindle (arrow) surrounded by chromosomes. H, mitotic U2OS cell expressing CENP-B–EGFP (kinetochore). Kinetochore spots of 500 nm or less were resolved. A–D acquired at 20×; E–H acquired at 20×, 8.5× zoom. Scale bar (H) applies to all images.

magnification, kinetochore fibers and spindle poles were well resolved (Fig. 2E), showing that critical mitotic structures can be studied *in vivo* by using the IVM methods developed here; HT-1080 cells expressing H2b–EGFP or β1-tubulin–TagRFP gave comparable images.

To test our ability to discriminate morphologies associated with drug-induced perturbations, HeLa cells in culture were pretreated with 2 drugs that induce morphologically distinct mitotic arrests, injected into DSCs, and imaged (Fig. 2F and G). Ptx-treated mitotic cells exhibited distributed rosettes of microtubules and scattered chromosomes (Fig. 2F), whereas K5I-treated cells (36) exhibited characteristic monopolar spindles (Fig. 2G). Our ability to robustly distinguish the 2 different mitotic arrest phenotypes shows that IVM has sufficient resolution to discriminate between related but distinct mitotic defects. As a more stringent test of resolution, U2OS cells expressing the centromeric protein CENP-B fused to EGFP were imaged. In either interphase (not shown) or mitotic cells, single CENP-B spots ($\leq$500 nm in size) were routinely resolved, which is consistent with the calculated diffraction limited resolution of our standard optics ($\sim$250 nm). From these initial data, normal and mitotic arrest structures appear identical in culture and *in vivo*, and we conclude that our cell models and methods will permit the identification of different mitotic spindle structures and the imaging of chromosomes, as condensed human chromosomes are typically several microns in length.

To evaluate tubulin imaging as a drug response marker *in vivo*, HT-1080 cells expressing β1-tubulin–TagRFP were used (Supplementary Fig. S1). Without Ptx, normal interphase and mitotic cells were observed. After 30 mg/kg Ptx treatment, mitotic arrest with microtubule rosettes was observed in a subset of cells, confirming drug delivery and drug action on these cells (Supplementary Fig. S1C–E). Although tubulin imaging allowed visualization of mitosis and confirmation of Ptx action, fluorescent histone H2b imaging reports on more features of drug response, including mitotic spindle structures, chromosome behavior, mitotic arrest and slippage, and cell death, and was therefore used in all subsequent experiments.

High-dose Ptx effects

Because multiple mitotic structures and chromosomes could be resolved in DSCs, we used IVM to assay PD (IPDM) in HT-1080 xenograft tumors. Tumors in Ptx-treated (single bolus of 30 mg/kg Ptx) mice showed few remaining tumors cells at day 17 (Supplementary Fig. S2A–D), in contrast to the vigorous tumors in saline-injected mice (not shown), indicating our model is highly sensitive to Ptx. Time-lapse z-series were collected at multiple random locations to reveal details of mitosis before and after drug. Time-lapse imaging was limited to 4 hours to minimize stress on the animals. Pre–drug treatment, we observed many examples of normal mitosis, but almost no examples of apoptosis (Supplementary Movie 2). The average duration of mitosis was 1 hour 6 minutes $\pm$ 6 minutes, which is remarkably comparable with these cells in culture, 1 hour 18 minutes $\pm$ 13 minutes. Nineteen hours post–Ptx treatment, the mitotic index was noticeably increased and cells that entered mitosis during the time-lapse imaging remained arrested (Fig. 3A–E; Supplementary Movie 3). Few cells died during mitotic arrest (not shown), and no cells divided. Arrested cells often slipped from mitotic arrest and became multinucleated (Fig. 3F–J). Multinucleated cells did not reenter mitosis but did die sometimes (Fig. 3B–E, I, and J; Supplementary Movies 3 and 4). The morphology of cell death, during mitosis or from a multinucleated state, resembled apoptosis, with chromatin condensation into multiple foci. Apoptotic bodies initially increased after Ptx treatment (not shown) but did not accumulate over time, presumably due to macrophage clearance. The 2 image

Downloaded from cancerres.aacrjournals.org on July 19, 2012
Copyright © 2011 American Association for Cancer Research

Published OnlineFirst June 30, 2011; DOI:10.1158/0008-5472.CAN-11-0412

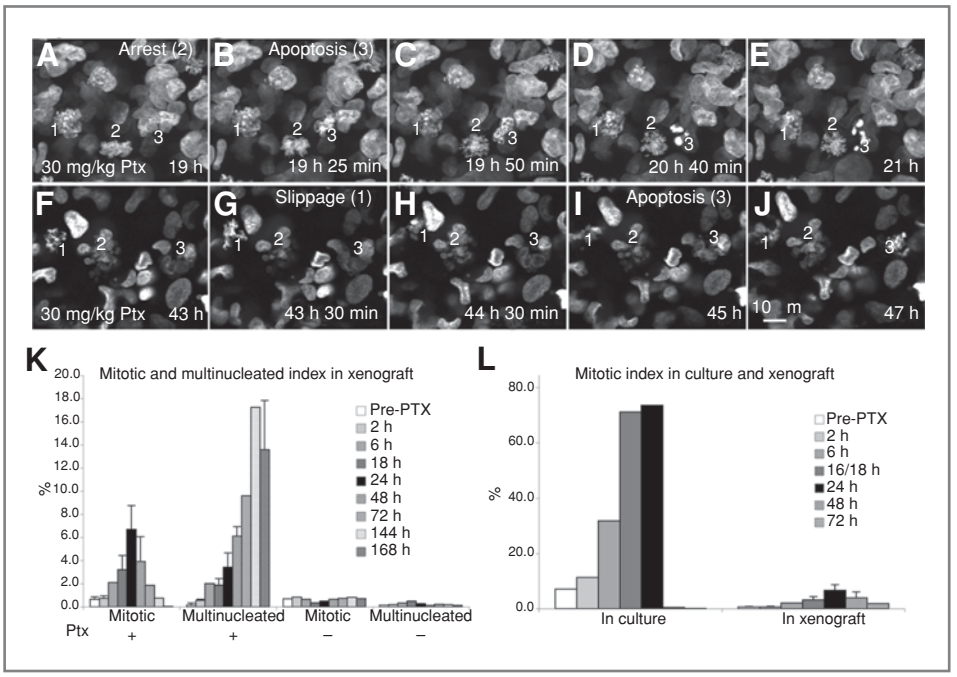

Figure 3. Time-lapse microscopy and analysis of mitotic events following saturating Ptx concentrations. A total of 30 mg/kg Ptx was used. A–E, cells 19 hours post–Ptx treatment. See Supplementary Movie 3. A, cell 1 is arrested, cell 2 is in early arrest, cell 3 is in postslippage phase. B, 25 minutes later, cell 3 died. C–E, cells 1 and 2 remained arrested. The DNA in cell 3 becomes condensed. F–J, same tumor, 43 hours post–Ptx treatment. See Supplementary Movie 4. F, cell 1 is arrested; cells 2 and 3 are multinucleated. G–J, 30 minutes later, cell 1 slipped from arrest and persisted. F–J, cell 2 remained multinucleated. Cell 3 died at approximately 45 hours post–Ptx treatment. K, *in vivo* analysis of mitotic and multinucleated index. The peak mitotic index was approximately 7% at 24 hours and decreased to below pre–Ptx treatment levels by 168 hours. The multinucleated index increased subsequent to mitotic index and remained elevated. L, comparison of indices in culture and *in vivo*. The pre–Ptx mitotic index in culture is higher than the xenograft and peaked at approximately 75% at 24 hours after Ptx treatment compared with approximately 7% at 24 hours in the xenograft. In culture, 240 cells were tracked. *In vivo*, more than 1,000 cells were scored for each time point. Time-lapse z-series acquired at 25×, 1.5× zoom. Scale bar (J) applies to all images.

sequences in Figure 3A–E and F to J are from the same tumor, illustrating how cell populations in the same tumor can be imaged repeatedly over time to capture the dynamics of drug response.

The Ptx response was quantified by measuring mitotic and multinucleated index as a function of time (Fig. 3K). Mitotic index increased from about 1.0% pre–Ptx treatment to about 7% maximum at 24 hours and then declined, reproducibly falling below baseline and reaching 0 at 168 hours (Fig. 3K). The multinucleated index increased, peaked later than the mitotic index, and reached higher levels (~17%) presumably because multinucleation is persistent, lasting days in some cases, whereas mitotic arrest is transient, lasting hours (Fig. 3K). To compare PD measures *in vivo* and in culture, we scored Ptx effects on HT-1080 cells in culture by continuous time-lapse imaging (21). The control pre–Ptx mitotic index was approximately 7% in culture (Fig. 3L) and at saturating Ptx concentrations (100 nmol/L), mitotic arrest peaked at 24 hours, with approximately 75% arrest. By 48 hours Ptx treatment, more than 90% of cells were dead (Supplementary Fig. S3A). In contrast to the situation in tumors, approximately 95% of mitosis-arrested cells in culture initiated apoptosis without slipping from mitosis and only about 5% slipped into the multinucleated G_1 state before dying (Supplementary Fig. S3; Supplementary Movie 5). Death directly from mitotic arrest is characteristic of apoptosis sensitive cells in culture (37).

Mitotic defects at low Ptx concentrations

To test whether IPDM could resolve subtle mitotic defects, including chromosome missegregation and multipolar mitoses, and to explore the utility of morphology as a quantitative PD marker, we also examined lower Ptx doses. At 1.2 mg/kg, most mitotic cells showed no morphologic defects ($n = 199$). At 3 mg/kg, mitotic cells appeared normal in single, static images. Time-lapse imaging, however, revealed frequent defects. Mitosis often required more than 2 hours to complete, significantly longer than in untreated tumors (~1 hour). Figure 4A–C (Supplementary Movie 6) shows a representative cell in which the metaphase spindle took abnormally long (>2 hours) to assemble and a chromosome–chromosome pair failed to align properly (Fig. 4D, arrow, inset). Several stretched, lagging chromosomes were also evident at anaphase (Fig. 4E–G; Supplementary Movie 6). These defects in chromosome segregation indicate abnormalities in kinetochore attachment and are frequently observed in cultured cells at low Ptx concentrations (31, 32). These data clearly show that time-lapse IPDM can reveal time-dependent mitotic phenotypes that are missed in single, static images.

Downloaded from cancerres.aacrjournals.org on July 19, 2012
Copyright © 2011 American Association for Cancer Research

Published OnlineFirst June 30, 2011; DOI:10.1158/0008-5472.CAN-11-0412

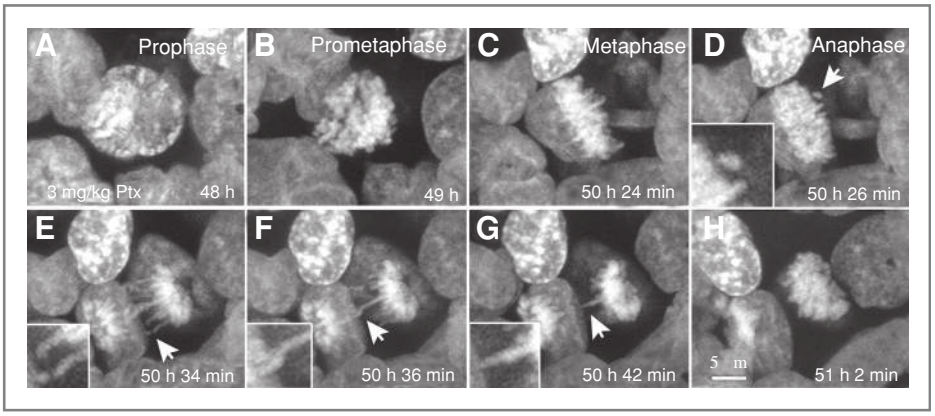

Figure 4. Low-dose Ptx results in mitotic delay and chromosome missegregation. Forty-eight hours after 3 mg/kg Ptx, a cell in prophase was imaged at 2-minute intervals, using a 60×, NA 1.10 water immersion lens. See Supplementary Movie 6. A–C, this cell required 2 hours 24 minutes to reach metaphase; the last frame before anaphase. D, upon anaphase, a single chromosome or chromosome pair progressed poleward separately from the others (arrow, inset). E–G, additional chromosomes were stretched during anaphase. H, this cell required 3 hours or more to complete mitosis, 2-fold longer than normal. Scale bar (H) applies to all images.

The mitotic phenotype at 3 mg/kg was mitotic delay and lagging chromosomes, so we increased the dose to 6 mg/kg to test whether we could induce spindle multipolarity as observed in culture at medium concentrations. In mice exposed to 6 mg/kg Ptx and imaged 2 to 4 hours after dosing, dividing cells entered anaphase frequently with lagging chromosomes, sometimes resulting in daughter cells with micronuclei (Fig. 5A; Supplementary Movie 7). By 24 hours, the mitotic index was increased and many mitotic cells were multipolar, with some cells dividing into 3 or more daughters (Fig. 5B; Supplementary Movie 8). These data suggest that the effective concentration of Ptx in tumor cells increased and remained high from 2 to 24 hours, consistent with previous PK data (27). There appeared to be considerable cell-to-cell

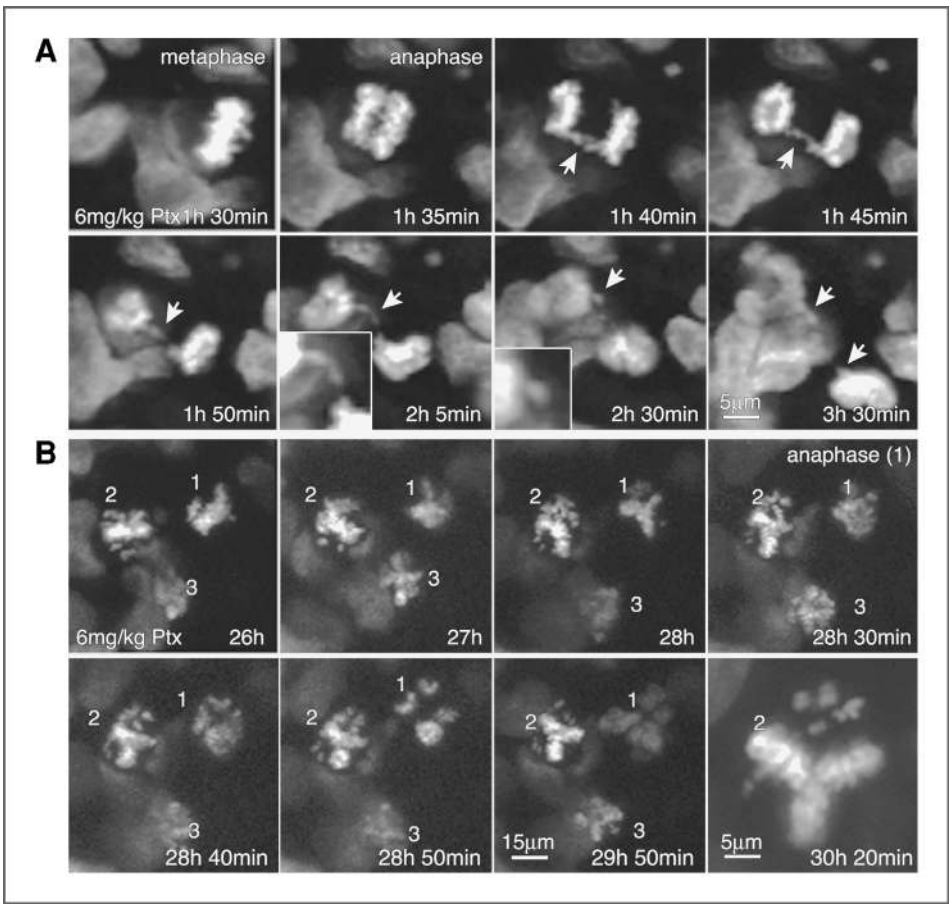

Figure 5. *In vivo* time lapse reveals PD principles of Ptx. A total of 6 mg/kg Ptx was used. A, after 1 hour 30 minutes Ptx treatment, a late prometaphase cell was imaged. This cell enters anaphase and initially appeared normal. Lagging chromosomes (arrows, inset) were present that subsequently resulted in micronucleus formation (arrows, insets, Supplementary Movie 7). B, multipolar mitosis occurs after 6 mg/kg Ptx. At 26 hours Ptx treatment, time lapse of random areas was done. See Supplementary Movie 8. Three cells (1, 2, and 3) are initially mitotic. By 28 hours, cell 1 is multipolar whereas cells 2 and 3 are arrested. Cell 1 underwent multipolar anaphase, cell 2 progressed toward a multipolar alignment, and cell 3 remained arrested. High magnification of cell 2 at 30 hours 20 minutes Ptx shows unaligned chromosomes. Note: It required more than 4 hours for cell 2 to become multipolar, indicating mitotic progression is delayed. Time-lapse z-series acquired at 25×, 1.5× zoom.

Downloaded from cancerres.aacrjournals.org on July 19, 2012
Copyright © 2011 American Association for Cancer Research

Published OnlineFirst June 30, 2011; DOI:10.1158/0008-5472.CAN-11-0412

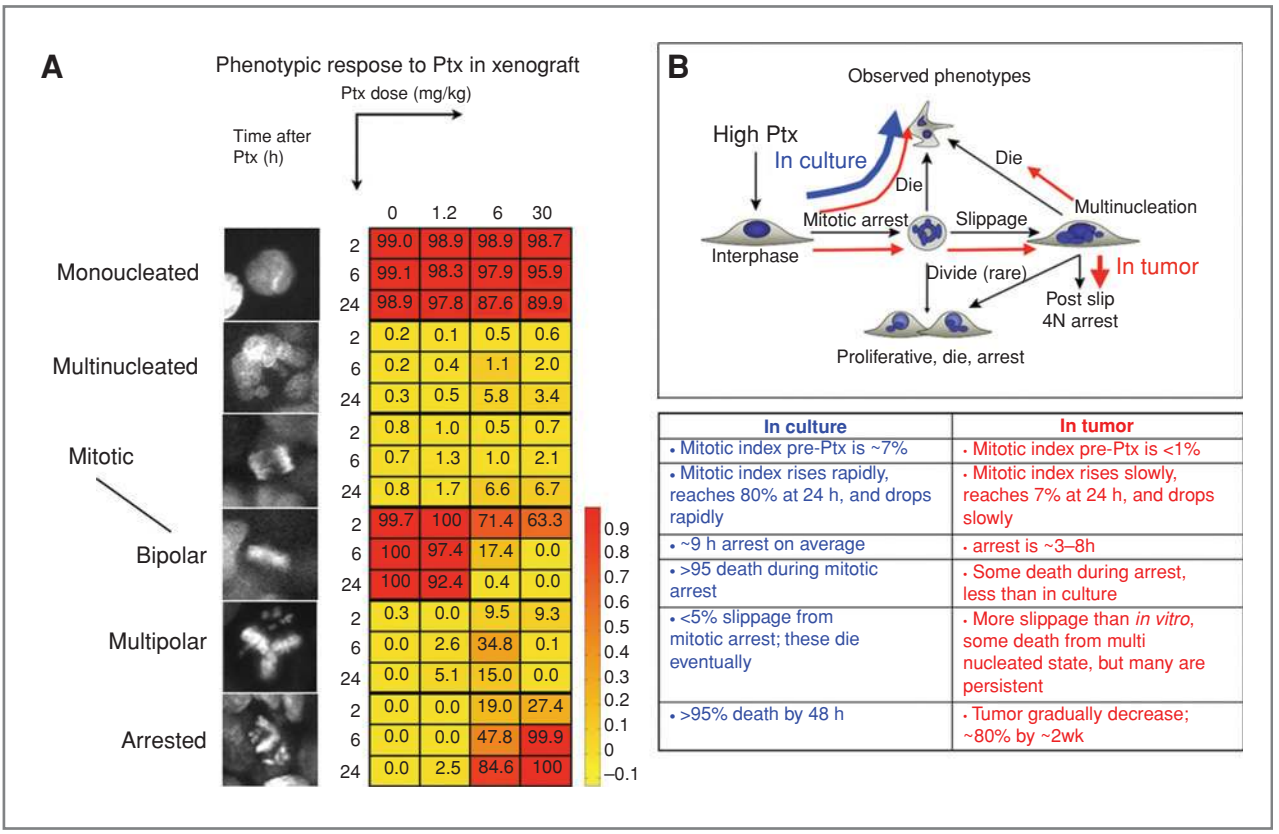

In culture	In tumor
• Mitotic index pre-Ptx is ~7%	• Mitotic index pre-Ptx is <1%
• Mitotic index rises rapidly, reaches 80% at 24 h, and drops rapidly	• Mitotic index rises slowly, reaches 7% at 24 h, and drops slowly
• ~9 h arrest on average	• arrest is ~3–8h
• >95 death during mitotic arrest	• Some death during arrest, less than in culture
• <5% slippage from mitotic arrest; these die eventually	• More slippage than *in vitro*, some death from multi nucleated state, but many are persistent
• >95% death by 48 h	• Tumor gradually decrease; ~80% by ~2wk

Figure 6. IPDM can be used to establish Ptx-PD over time and dose, and Ptx response is significantly different *in vivo* than in culture. A, phenotypic responses are color coded in response to increasing doses of Ptx at 2, 6, and 24 hours treatment. The majority of cells remained mononucleated during the first 24 hours and both 6 and 30 mg/kg showed increasing multinucleated and mitotic indices. To establish PD of Ptx on mitosis, mitotic profiles were further separated to include bipolar, multipolar, and arrested phenotypes. As the percentage of bipolar cells decreases, the multipolar and arrested phenotypes increase. For 1.2 mg/kg Ptx, a small increase in multipolarity and arrest occurred at 24 hours. For 6 mg/kg, by 6 hours, more than 30% of cells were multipolar, which remained at 15% at 24 hours; the percentage of arrested cells steadily increased at 24 hours. Unlike 1.2 and 6 mg/kg, 30 mg/kg did not accumulate or maintain significant multipolarity. After 2 hours, the percentage of multipolar cells sharply decreased and all mitotic stages displayed an arrested phenotype. B, summary of in-culture and in-tumor responses to saturating Ptx concentrations.

variability in tumors at 6 mg/kg, in contrast to the uniform mitotic arrest observed at 30 mg/kg.

Mitotic morphology as a PD marker

We used IPDM to quantify mitotic morphology as a function of dose and time up to 24 hours to determine whether phenotype could be used as an effective measure of the Ptx concentration (Fig. 6A). Normal mitosis decreased and mitotic abnormalities increased with dose and time. Interestingly, multinucleated cells and multipolar mitoses peaked at intermediate doses (6 mg/kg) and times (6 hours), showing that these morphologies report on exposure of cells to nonsaturating drug concentrations. For high-dose Ptx, multipolar mitoses peak at 2 hours, indicating that Ptx had not reached saturation, but it had by 6 hours, as all mitotic cells were then arrested (Fig. 6A). The PD of Ptx during the first 24 hours in saturating conditions was dramatically different in tumors than in culture (Supplementary Fig. S4). In culture, by 2 hours, all mitotic cells showed the arrested phenotype, the mitotic index increased rapidly, and there was little multinucleation and by 24 hours 70% of cells were dead. In tumors, there was a delay in mitotic arrest phenotype, the mitotic index increased, but remained comparatively low, and there was little death by 24 hours. These data show that Ptx PD is significantly different in these tumors than in culture and IPDM can be used to characterize the Ptx concentration experienced by individual cells in tumors over time.

Discussion

Using optimized microscopic and animal preparations, we show that normal mitosis and antimitotic drug responses can be visualized at subcellular ($\leq$500 nm) spatial resolution *in vivo* (Fig. 2). The data show that the power of IPDM to reveal detailed aspects of mitosis, mitotic abnormalities, and drug PD in tumors. These methods should be equally applicable to any organ that can be imaged using a window chamber or exteriorized, and perhaps to internal organs/tumors, using multiphoton microscopy. Furthermore, the general methods can be tailored using specific probes to study many different pathways in disease and cell biology *in vivo*. Using IPDM, we gained new insights into Ptx PD in a tumor model that are

Downloaded from cancerres.aacrjournals.org on July 19, 2012
Copyright © 2011 American Association for Cancer Research

Published OnlineFirst June 30, 2011; DOI:10.1158/0008-5472.CAN-11-0412

summarized in Figure 6B for the saturating 30 mg/kg dose, wherein we compare the effects of continuous exposure to saturating Ptx concentrations on the same cells in culture. The lower peak of mitotic arrest in tumors is consistent with a slower proliferation rate, but because the peak mitotic arrest occurred at 24 hours in both cases, the cell-cycle transit time for cells that commit to divide must be similar. The low-peak mitotic arrest in HT-1080 tumors resembles the response seen in other mouse cancer models by histology of tumor sections and in human breast cancers by histology of fine needle aspirates (16, 29, 38). Mitosis-arrested cells tended to slip in tumors and to die directly from mitotic arrest in culture. Presumably, this reflects enhanced prosurvival signaling in the tumor, which allows slippage to win the kinetic competition with apoptosis induction (19, 39).

PK studies of Ptx in mice showed that upon bolus i.v. injection at 40 mg/kg, plasma levels peaked within 5 minutes (27, 34) but remained detectable for 14 days or more (34). Ptx has also been reported to be detectable within minutes of injection in an s.c. lung xenograft, and several tissues reach its peak concentration by approximately 2 hours and remain detectable in these tissues for 14 days or more (34). Our PD data for 30 mg/kg Ptx agree well with these PK data as we observed mitotic arrest, indicating effective Ptx reaching the tumors by 2 hours (Fig. 6, images not shown). The published half-life of Ptx (based on concentration determined using tritylated Ptx and high-performance liquid chromatography) in mouse tissues and lung xenograft tumors after a 40 mg/kg dose was reported as approximately 50 to 70 hours (34), and our PD data at 30 mg/kg show that Ptx remained maximally effective at 72 hours, as all mitotic cells at this time were arrested. Furthermore, at 72 hours Ptx remains high in the tumors because if washed away, mitotic cells would be either normal or multipolar, although this was not observed. From 72 to 168 hours post–Ptx treatment, we noted a dramatic decrease in mitotic cells (Fig. 3K) and did not trap any dividing cells with a second dose of 30 mg/kg Ptx at 168 hours after the first dose (not shown). These observations suggest that the remaining tumor cells are no longer proliferating despite the fact that they are mostly mononucleated, implying that they have not divided in Ptx. Ptx either damaged the remaining cells in a manner that is not evident from H2b–EGFP imaging or the tumor microenvironment has changed so that it no longer supports proliferation. This change is long-lasting in that xenograft tumors showed significant regression by 2 weeks (Supplementary Fig. S2). Consistent with these ideas, Symmans and colleagues found some human breast cancers that showed only a modest increase in mitotic index and little cell death in the first 48 hours after Ptx treatment, but these tumors later converted to a "sustained apoptotic response" 16). Elucidating how a modest mitotic arrest results in minimal cell killing in some tumors but translates into a sustained response with significant tumor clearance in others could be useful for improving antimitotic therapy.

The dose- and time-dependent effects revealed by IPDM show its potential to report on single-cell biomarkers. Tumors are genetically and environmentally heterogeneous, and individual cancer cells can respond differently to drugs even in culture (19, 21, 40). Cell-to-cell and intratumor heterogeneity are likely in tumors. Thus, PD biomarkers with subcellular resolution may prove very valuable in understanding drug responses. Furthermore, on the basis of our results with low-dose Ptx, it should be possible to visualize and quantify chromosome segregation defects that contribute to cancer progression in a tumor context, using IPDM, which is unique in its ability to reveal a dynamic response to drugs at the single-cell level and allows for the use of many different probes, including fluorescent dyes, particles, and antibodies, and probes for specific activities including kinases and proteases (1, 12, 41). In this study, a chromatin marker allowed us to study normal and abnormal mitotic progression in real time at the resolution of single chromosomes, to monitor single cells responding to drug and undergoing apoptosis, and to establish drug PD over dose and time. The features of IPDM create a powerful technique with a bright future.

Disclosure of Potential Conflicts of Interest

No potential conflicts of interest were disclosed.

Acknowledgments

The authors thank Jose-Luiz Figueiredo and Rostic Gorbatov for help with mice, Soyeon Park for editorial assistance, the Center for Systems Biology platform for *in vivo* microscopy, and the Nikon Imaging Center at Harvard Medical School.

Grant Support

This study was funded by NIH grants CA139980 (to T.J. Mitchison), CA084179 (to P.K. Sorger), and CA86355 and CA092782 (to R. Weissleder).

The costs of publication of this article were defrayed in part by the payment of page charges. This article must therefore be hereby marked *advertisement* in accordance with 18 U.S.C. Section 1734 solely to indicate this fact.

Received February 7, 2011; revised May 6, 2011; accepted May 11, 2011; published OnlineFirst June 28, 2011.

References

1. Weissleder R, Pittet MJ. Imaging in the era of molecular oncology. Nature 2008;452:580–9.
2. Falkvoll KH, Rofstad EK, Brustad T, Marton P. A transparent chamber for the dorsal skin fold of athymic mice. Exp Cell Biol 1984;52:260–8.
3. Lehr HA, Leunig M, Menger MD, Nolte D, Messmer K. Dorsal skinfold chamber technique for intravital microscopy in nude mice. Am J Pathol 1993;143:1055–62.
4. Brown DL, Meagher PJ, Knight KR, Keramidaris E, Romeo-Meeuw R, Penington AJ, et al. Survival and function of transplanted islet cells on an *in vivo*, vascularized tissue engineering platform in the rat: A pilot study. Cell Transplant 2006;15:319–24.
5. Fiorina P, Jurewicz M, Tanaka K, Behazin N, Augello A, Vergani A, et al. Characterization of donor dendritic cells and enhancement of dendritic cell efflux with CC-chemokine ligand 21: a novel strategy to prolong islet allograft survival. Diabetes 2007;56:912–20.
6. Kedrin D, Gligorijevic B, Wyckoff J, Verkhusha VV, Condeelis J, Segall JE, et al. Intravital imaging of metastatic behavior through a mammary imaging window. Nat Methods 2008;5:1019–21.

Downloaded from cancerres.aacrjournals.org on July 19, 2012
Copyright © 2011 American Association for Cancer Research

Published OnlineFirst June 30, 2011; DOI:10.1158/0008-5472.CAN-11-0412

7. Makale M. Intravital imaging and cell invasion. Methods Enzymol 2007;426:375–401.
8. Wyckoff JB, Wang Y, Lin EY, Li JF, Goswami S, Stanley ER, et al. Direct visualization of macrophage-assisted tumor cell intravasation in mammary tumors. Cancer Res 2007;67:2649–56.
9. Brown E, Munn LL, Fukumura D, Jain RK. *In vivo* imaging of tumors. Cold Spring Harb Protoc 2010;2010:pdb.prot5452.
10. Gualda EJ, Filippidis G, Mari M, Voglis G, Vlachos M, Fotakis C, et al. *In vivo* imaging of neurodegeneration in *Caenorhabditis elegans* by third harmonic generation microscopy. J Microsc 2008;232:270–5.
11. Yaniv K, Isogai S, Castranova D, Dye L, Hitomi J, Weinstein BM. Live imaging of lymphatic development in the zebrafish. Nat Med 2006;12:711–6.
12. Weigert R, Sramkova M, Parente L, Amornphimoltham P, Masedunskas A. Intravital microscopy: a novel tool to study cell biology in living animals. Histochem Cell Biol 2010;133:481–91.
13. Sen S. Aneuploidy and cancer. Curr Opin Oncol 2000;12:82–8.
14. Jackson JR, Patrick DR, Dar MM, Huang PS. Targeted anti-mitotic therapies: can we improve on tubulin agents? Nat Rev Cancer 2007; 7:107–17.
15. Woods CM, Zhu J, McQueney PA, Bollag D, Lazarides E. Taxol-induced mitotic block triggers rapid onset of a p53-independent apoptotic pathway. Mol Med 1995;1:506–26.
16. Symmans WF, Volm MD, Shapiro RL, Perkins AB, Kim AY, Demaria S, et al. Paclitaxel-induced apoptosis and mitotic arrest assessed by serial fine-needle aspiration: implications for early prediction of breast cancer response to neoadjuvant treatment. Clin Cancer Res 2000;6: 4610–7.
17. Sugimura M, Sagae S, Ishioka S, Nishioka Y, Tsukada K, Kudo R. Mechanisms of paclitaxel-induced apoptosis in an ovarian cancer cell line and its paclitaxel-resistant clone. Oncology 2004;66:53–61.
18. Soma D, Kitayama J, Ishigami H, Kaisaki S, Nagawa H. Different tissue distribution of paclitaxel with intravenous and intraperitoneal administration. J Surg Res 2009;155:142–6.
19. Gascoigne KE, Taylor SS. Cancer cells display profound intra- and interline variation following prolonged exposure to antimitotic drugs. Cancer Cell 2008;14:111–22.
20. Brito DA, Rieder CL. Mitotic checkpoint slippage in humans occurs via cyclin B destruction in the presence of an active checkpoint. Curr Biol 2006;16:1194–200.
21. Orth JD, Tang Y, Shi J, Loy CT, Amendt C, Wilm C, et al. Quantitative live imaging of cancer and normal cells treated with Kinesin-5 inhibitors indicates significant differences in phenotypic responses and cell fate. Mol Cancer Ther 2008;7:3480–9.
22. Schiff PB, Horwitz SB. Taxol stabilizes microtubules in mouse fibroblast cells. Proc Natl Acad Sci U S A 1980;77:1561–5.
23. Hadfield JA, Ducki S, Hirst N, McGown AT. Tubulin and microtubules as targets for anticancer drugs. Prog Cell Cycle Res 2003;5:309–25.
24. Orr GA, Verdier-Pinard P, McDaid H, Horwitz SB. Mechanisms of Taxol resistance related to microtubules. Oncogene 2003;22:7280–95.
25. Ishigami H, Kitayama J, Otani K, Kamei T, Soma D, Miyato H, et al. Phase I pharmacokinetic study of weekly intravenous and intraperitoneal paclitaxel combined with S-1 for advanced gastric cancer. Oncology 2009;76:311–4.
26. Eiseman JL, Eddington ND, Leslie J, MacAuley C, Sentz DL, Zuhowski M, et al. Plasma pharmacokinetics and tissue distribution of paclitaxel in CD2F1 mice. Cancer Chemother Pharmacol 1994;34:465–71.
27. Dhanikula AB, Singh DR, Panchagnula R. *In vivo* pharmacokinetic and tissue distribution studies in mice of alternative formulations for local and systemic delivery of paclitaxel: gel, film, prodrug, liposomes and micelles. Curr Drug Deliv 2005;2:35–44.
28. Milross CG, Mason KA, Hunter NR, Chung WK, Peters LJ, Milas L. Relationship of mitotic arrest and apoptosis to antitumor effect of paclitaxel. J Natl Cancer Inst 1996;88:1308–14.
29. Milas L, Hunter NR, Kurdoglu B, Mason KA, Meyn RE, Stephens LC, et al. Kinetics of mitotic arrest and apoptosis in murine mammary and ovarian tumors treated with Taxol. Cancer Chemother Pharmacol 1995;35:297–303.
30. Chakravarthy A, Nicholson B, Kelley M, Beauchamp D, Johnson D, Frexes-Steed M, et al. A pilot study of neoadjuvant paclitaxel and radiation with correlative molecular studies in stage II/III breast cancer. Clin Breast Cancer 2000;1:68–71.
31. Ikui AE, Yang CP, Matsumoto T, Horwitz SB. Low concentrations of Taxol cause mitotic delay followed by premature dissociation of p55CDC from Mad2 and BubR1 and abrogation of the spindle checkpoint, leading to aneuploidy. Cell Cycle 2005;4:1385–8.
32. Martinez-Exposito MJ, Kaplan KB, Copeland J, Sorger PK. Retention of the BUB3 checkpoint protein on lagging chromosomes. Proc Natl Acad Sci U S A 1999;96:8493–8.
33. Alexander S, Koehl GE, Hirschberg M, Geissler EK, Friedl P. Dynamic imaging of cancer growth and invasion: a modified skin-fold chamber model. Histochem Cell Biol 2008;130:1147–54.
34. Wang X, Zhao G, Van S, Jiang N, Yu L, Vera D, et al. Pharmacokinetics and tissue distribution of PGG-paclitaxel, a novel macromolecular formulation of paclitaxel, in nu/nu mice bearing NCI-460 lung cancer xenografts. Cancer Chemother Pharmacol 2010;65: 515–26.
35. Mason KA, Milas L, Peters LJ. Effect of paclitaxel (Taxol) alone and in combination with radiation on the gastrointestinal mucosa. Int J Radiat Oncol Biol Phys 1995;32:1381–9.
36. Schiemann K, Finsinger D, Zenke F, Amendt C, Knochel T, Bruge D, et al. The discovery and optimization of hexahydro-2*H*-pyrano[3,2-*c*]quinolines (HHPQs) as potent and selective inhibitors of the mitotic kinesin-5. Bioorg Med Chem Lett 2010;20:1491–5.
37. Shi J, Orth JD, Mitchison T. Cell type variation in responses to antimitotic drugs that target microtubules and kinesin-5. Cancer Res 2008;68:3269–76.
38. Symmans FW. Breast cancer response to paclitaxel *in vivo*. Drug Resist Updat 2001;4:297–302.
39. Huang HC, Shi J, Orth JD, Mitchison TJ. Evidence that mitotic exit is a better cancer therapeutic target than spindle assembly. Cancer Cell 2009;16:347–58.
40. Yang R, Niepel M, Mitchison TJ, Sorger PK. Dissecting variability in responses to cancer chemotherapy through systems pharmacology. Clin Pharmacol Ther 2010;88:34–8.
41. Zhou F, Xing D, Wu S, Chen WR. Intravital imaging of tumor apoptosis with FRET probes during tumor therapy. Mol Imaging Biol 2009;12: 63–70.

Downloaded from cancerres.aacrjournals.org on July 19, 2012
Copyright © 2011 American Association for Cancer Research